Effect of annealing on the physical properties of thermally evaporated In$_2$S$_3$ thin films

S. Rasool[a], K. Saritha[a], K.T. Ramakrishna Reddy[a,*], M.S. Tivanov[b], A.V. Trofimova[b], S.E. Tikoto[b], L. Bychto[c], A. Patryn[c], M. Maliński[c], V.F. Gremenok[d]

[a] *Solar Photovoltaic Laboratory, Department of Physics, Sri Venkateswara University, Tirupati, 517 502, Andhra Pradesh, India*
[b] *Department of Energy Physics, Belarusian State University, Nezavisimosti 4 Av., 220030, Minsk, Belarus*
[c] *Department of Electronics & Computer Sciences, Koszalin University of Technology, Koszalin, 75-453, Poland*
[d] *Scientific and Practical Materials Research Centre, National Academy of Sciences, 220072, Minsk, Belarus*

A B S T R A C T

The structural, compositional, morphological and optical properties of In$_2$S$_3$ thin films, prepared by thermal evaporation technique and annealed in sulfur ambient at different temperatures have been investigated. The grazing incident X-ray diffraction patterns have indicated polycrystalline form and predominantly cubic structure of annealed In$_2$S$_3$ films. The scanning electron microscopy revealed textured surface with uniformly distributed grains and the grain size increased with increase of annealing temperature. The optical parameters of the films have been determined using conventional transmission and reflection spectra as well as from surface photovoltage measurements.

1. Introduction

Indium sulfide (In$_2$S$_3$) is a III-VI semiconductor with an n-type electrical conductivity and a wide direct energy band gap of ~2.2 eV [1–3]. Due to its good photoconductive properties, high transparency in the visible spectral region and chemical stability, In$_2$S$_3$ thin films were appeared to be suitable to use as a buffer or window layer in thin film solar cells instead of cadmium sulfide (CdS) [4–6]. In$_2$S$_3$ thin films have been deposited on different substrates (ITO, FTO, etc.) using various deposition techniques such as atomic layer deposition (ALD), physical vapour deposition (PVD), ultrasonic spray pyrolysis (USP), chemical spray pyrolysis (CSP), sputtering, atomic layer epitaxy (ALE), ionic layer gas atomic reaction (ILGAR), electrodeposition (ED), chemical bath deposition (CBD) and metal organic chemical vapour deposition (MOCVD) [1]. The maximum solar conversion efficiency of 16.4% has been demonstrated by using In$_2$S$_3$ buffer layer in Cu(In,Ga)Se$_2$-based thin film solar cells [5,6], that is close to the value 20% achieved using CdS as buffer layer in these cells [7,8].

In general, the material properties can be enhanced by either doping or annealing processes. During post-annealing process of thin films, recrystallization occurs, which causes improvement in crystallinity of the films and increases grain size depending up on the working temperature. Therefore, annealing of the films at optimized conditions could improve the film quality with reduced surface roughness and defects present in the films. Many research groups studied the annealing effect on physical properties of In$_2$S$_3$ thin films at various conditions. Some of the reports available on annealed In$_2$S$_3$ thin films on different substrates and at different conditions are listed in Table 1.

It should be noted that most of the information about optical parameters of In$_2$S$_3$ films are reported to be received by conventional optical transmission spectroscopy [22–25]. However, additional study of the evolution of these parameters by surface photovoltage (SPV) spectroscopy can be also useful here. The SPV is a non-destructive technique to study opto-electronic properties of semiconductor materials by measuring of the photoinduced changes in the surface voltage [26]. The surface voltage is known to be proportional to the concentration of charge carriers. During sample irradiation, the excess carriers are generated and in the course of diffusion and recombination processes, the carrier concentration distribution is changed, which leads to changes of surface potential. Based on the obtained SPV signal, the type of conductivity of the material also can be determined [27,28]. Besides, it is possible to identify different types of electronic transitions such as defect states-to-band, surface states-to-band and band-to-band transitions that occur in semiconducting materials and even for buried layers, hetero-structures and multi-phased nano structures with SPV technique, where conventional optical spectroscopic techniques are not

Table 1
Data of annealed In$_2$S$_3$ thin films presented in literature.

Deposition method	Annealing temperature (°C)	Annealing atmosphere	Phase	Structure	S/In ratio	Band gap (eV)	Ref.
Thermal evaporation	150	vacuum	β-In$_2$S$_3$	tetragonal	1.39–1.38	–	[9]
Thermal evaporation	100–400	vacuum	β-In$_2$S$_3$	tetragonal	1.25–1.75	1.5–2.9	[10]
			InS	cubic			
Thermal evaporation	200–350	air	β-In$_2$S$_3$	tetragonal	–	2.0–2.2	[11]
Thermal evaporation	150–450	air	β-In$_2$S$_3$	tetragonal	1.46	2.84–3.04	[12]
Thermal evaporation	250–350	nitrogen	β-In$_2$S$_3$	tetragonal	–	1.94–2.19	[13]
Thermal evaporation	150 & 200	vacuum	β-In$_2$S$_3$	tetragonal	1.39–1.38	2.65–2.75	[14]
Close space evaporation	100–500	vacuum	β-In$_2$S$_3$	tetragonal	0.96–0.82	2.41–2.18	[15]
Flash evaporation	100–420	vacuum, sulfur	β-In$_2$S$_3$	tetragonal	1.52–1.67	2.50–2.65	[16]
	100–400	vacuum	Mixed phases	tetragonal	0.56	2.4–1.5	[17]
Spray pyrolysis	100–400	air	β-In$_2$S$_3$	tetragonal	–	2.61–2.51	[18]
Modulated flux deposition	250 & 350	vacuum, sulfur	β-In$_2$S$_3$	tetragonal	1.4–1.6	2.66, 2.73	[19]
CBD	200–300	air	amorphous In$_2$S$_3$	–	–	3.0–2.0	[20]
CBD	400	nitrogen	β-In$_2$S$_3$	Cubic	–	–	[21]
Thermal evaporation	200–300	sulfur	β-In$_2$S$_3$	Cubic	1.05–1.66	1.90–2.71	Present work

applicable [29]. Therefore, in the present study, the changes occurred in the structural, morphological and optical properties of In$_2$S$_3$ layers upon their post deposition annealing at various temperatures were investigated and discussed. In particular, the optical properties were investigated using both conventional optical spectroscopy and surface photovoltage (SPV) spectroscopy measurements to evaluate the optical behaviour of the In$_2$S$_3$ films.

2. Experimental details

In$_2$S$_3$ thin films were grown by thermal evaporation technique (HHV BC300 model) at a constant substrate temperature (T$_s$) of 300 °C on ultrasonically cleaned soda lime glass substrates using In$_2$S$_3$ powder (Sigma Aldrich 99.999% purity) as source material. The as-grown films were annealed in sulfur ambient at a residual pressure of 2×10^{-2} mbar at various temperatures (T$_a$) in the range of 200 °C–300 °C for 1 h using a two zone tubular furnace. The structural characteristics of In$_2$S$_3$ films were analysed using Ultima IV X-ray diffractometer (Rigaku) in grazing incidence X-ray diffraction (GIXD) geometry at 1° of incident X-rays with CuK$_\alpha$ radiation source ($\lambda = 1.5406$ Å) scanned in the range of 10°–80°. The surface morphology of the films was investigated using Hitachi S-806 scanning electron microscope (SEM). The chemical composition of the films was obtained by energy dispersive x-ray spectroscopy (EDS). The transmission and reflection spectra of the films were measured using a Photon RT spectrophotometer (Essent Optics). The SPV signal was obtained in non-contact mode of metal-insulator-semiconductor (MIS) configuration, measured in the wavelength range of 400–700 nm at a constant frequency of modulation (226 Hz) [29].

3. Results and discussions

The as-grown and annealed In$_2$S$_3$ films were uniform, free from pinholes and cracks on the surface of the films and well-adherent to the substrate surface.

3.1. Structural analysis

Fig. 1 shows the GIXD patterns of as-grown and annealed In$_2$S$_3$ films, which exhibit polycrystalline nature of the films irrespective of the annealing temperatures.

For the as-grown films, the peaks obtained at 2θ = 24.96°, 32.83°, 38.69° and 46.36° are corresponding to (300), (400), (421) and (521) planes respectively, which are related to cubic β-In$_2$S$_3$ phase (JCPDS: 32-0456) with (300) plane as its preferred orientation. Also, certain minor peaks are observed at 2θ = 17.02° and 18.67° that are related to the (112) and (105) orientations respectively corresponding to

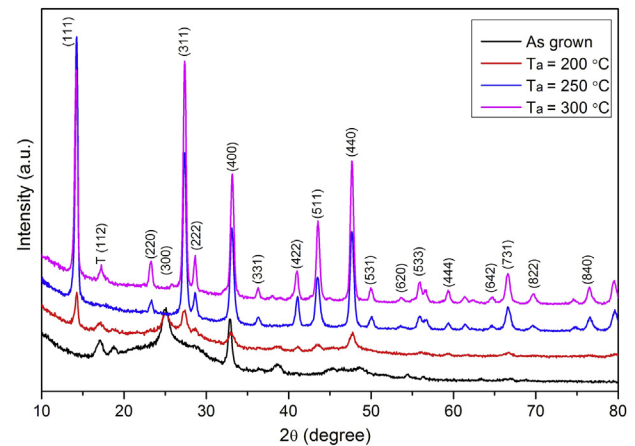**Fig. 1.** GIXD patterns of In$_2$S$_3$ films.

tetragonal β-In$_2$S$_3$ (JCPDS 73-1366). As seen from Fig. 1 the annealing of the films up to 250 °C leads to a presence of both orientations (111) and (311) of cubic phase, the intensity of (111) peak increases significantly compared to other peaks and the intensity of reflection of tetragonal phase decrease. This indicates an improvement in crystallinity of the films and suppression of tetragonal phase with an increase of annealing temperature [30]. But at 300 °C, the (112) reflection of tetragonal phase is observed again along with changes in preferred orientation of cubic phase from (111) to (311). It can be explained by the fact that the rate of grain growth can differ for crystallographic orientations of (111) and (311) due to anisotropy of the crystal. In this case even for high annealing temperatures the secondary tetragonal phase isn't suppressed completely. The existence of both cubic and tetragonal phases was also reported in several works for In$_2$S$_3$ layers prepared by different methods [31–33].

The structural parameters such as interplanar spacing (d), lattice constant (a), size of coherent scattering region (L), dislocation density (δ) and internal lattice strain (ε) were calculated according to the preferred (hkl) plane of as-grown and annealed In$_2$S$_3$ films using the following relations and the obtained values are presented in Table 2.

The interplanar spacing (d) was calculated using the Bragg's diffraction law:

$$d = \frac{n\lambda}{2 \sin \theta},\tag{1}$$

where n is an integer, λ is the wavelength of incident CuK$_\alpha$ radiation, θ is a Bragg angle. Since all the preferred orientations of In$_2$S$_3$ films were related to cubic structure, the lattice constant is 'a' (a = b = c) that can be calculated using the following equation:

Table 2
The structural parameters of In_2S_3 films.

T_a (°C)	2θ (°)	(hkl)	FWHM (radians)	d (Å)	a (Å)	L (nm)	δ (lines/m²)	$\varepsilon \times 10^{-2}$
As-grown	25.10	(300)	0.046141	3.54	10.62	3.0	1.09×10^{17}	5.54
200	14.25	(111)	0.008671	6.21	10.75	15.8	4.00×10^{15}	1.85
250	14.25	(111)	0.007626	6.21	10.75	18.0	3.09×10^{15}	1.63
300	27.35	(311)	0.008369	3.25	10.77	16.7	3.57×10^{15}	0.91

$$a = d\sqrt{h^2 + k^2 + l^2}. \tag{2}$$

The size of coherent scattering region was estimated by the Debye-Scherrer formula [34]:

$$L = \frac{0.94\lambda}{\beta cos\theta}, \tag{3}$$

where β is an integral breadth of the prevailing peak in radians. We use Gauss approximation of the peaks, when $\beta = \left(\frac{\pi}{4ln2}\right)^{1/2} \times FWHM$. FWHM is full width at peak half maximum height. The dislocation density was calculated using the Williamson-Smallman relation [35]:

$$\delta = \frac{1}{L^2} \tag{4}$$

The lattice deformation was calculated using the following relation [36]:

$$\varepsilon = \frac{\beta}{4 \tan \theta} \tag{5}$$

3.2. Elemental analysis

The elemental analysis of as-grown and annealed In_2S_3 films was carried out by employing energy dispersive spectroscopy (EDS). Fig. 2 shows the typical EDS spectrum of In_2S_3 films annealed at 250 °C and the elemental atomic percentages of 'In' and 'S' in the films with respect to annealing temperature are given in Table 3. In order to grow In_2S_3 thin films, the bulk material with an S/In ratio closed to stoichiometry was used. Upon thermal evaporation of the material the sulfur content decreased strongly due to its high volatility. The post annealing process carried in vacuum is known for an additional loss of sulfur due to re-

Table 3
EDS elemental analysis of In_2S_3 films.

T_a (°C)	Atomic content (%)		S/In
	In	S	
Bulk	40.20	59.80	1.49
As-grown	48.73	51.27	1.05
200	45.53	54.47	1.19
250	39.50	60.50	1.53
300	37.48	62.52	1.66

evaporation from the film [12,15]. To avoid such negative effect, the as-grown films were annealed in sulfur ambient, resulting to gradual increase of sulfur content in the films with an increase of annealing temperature (see Table 3). At higher annealing temperatures, a rapid reaction of S vapors with In led to the formation of stoichiometric β-In_2S_3 phase. So, films annealed at 250 °C showed a S/In ratio of 1.53, which is close to 1.49 of bulk In_2S_3 [14]. Bouabid et al. [16] also reported S/In value of 1.67 for flash evaporated In_2S_3 films annealed at 573 K under sulfur atmosphere. Such method of annealing allows to receive necessary S/In ratio in In_2S_3 films.

3.3. Morphological studies

Fig. 3(a–c) shows the SEM micrographs of annealed In_2S_3 layers at T_a = 200 °C, 250 °C and 300 °C. The SEM images showed that the films were free of pinholes, voids and cracks. It is observed from the SEM images that the surface of the films was distributed with large, uniform granular structure and well-defined grain boundaries. Further, the grain size of the films was increased with annealing temperature. This is
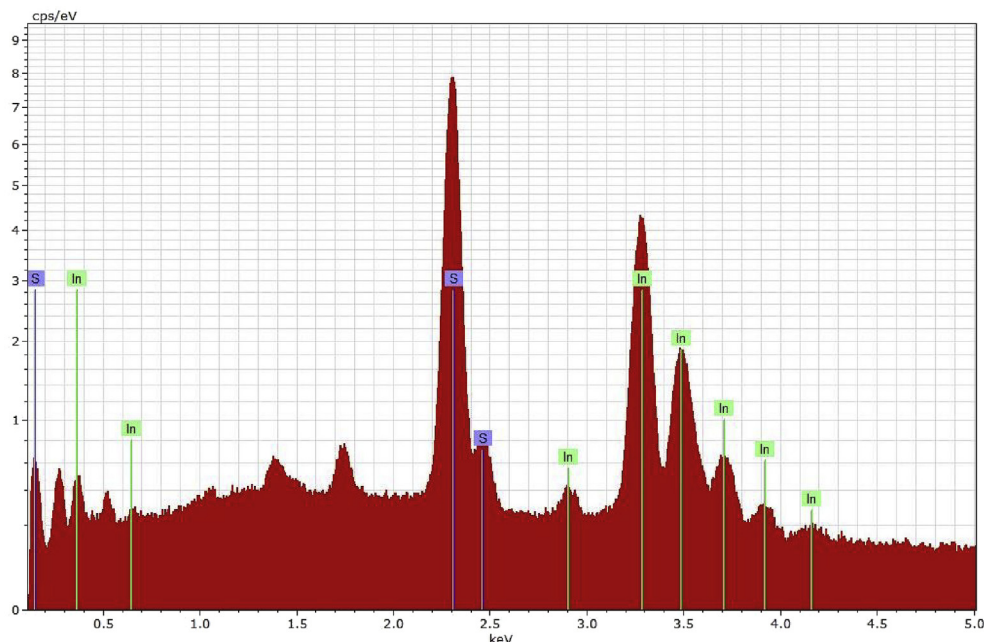

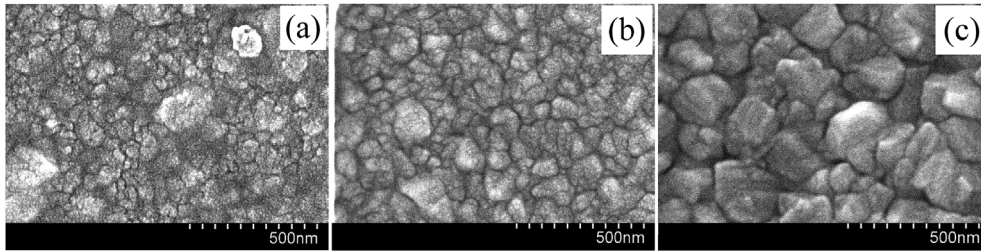**Fig. 2.** Typical EDS spectrum of In_2S_3 films annealed at T_a = 250 °C.

Fig. 3. SEM images of In₂S₃ films annealed at (a) T$_a$ = 200 °C; (b) T$_a$ = 250 °C; (c) T$_a$ = 300 °C.

mainly due to the coalescence of neighbouring grains at higher temperatures. In general, the grain size of the films was greatly influenced by the substrate temperature, annealing temperature and also thickness of the films [12,37]. The changes in grain size obviously depend on the annealing conditions applied and even the type of the sample. In the present analysis, the grain size of the In₂S₃ films was increased up on annealing, indicating the improved crystallinity of the layers, which was confirmed by the GIXD analysis.

3.4. Optical studies

Fig. 4 shows the optical transmission and reflection spectra for In₂S₃ films as-grown and annealed at different temperatures.

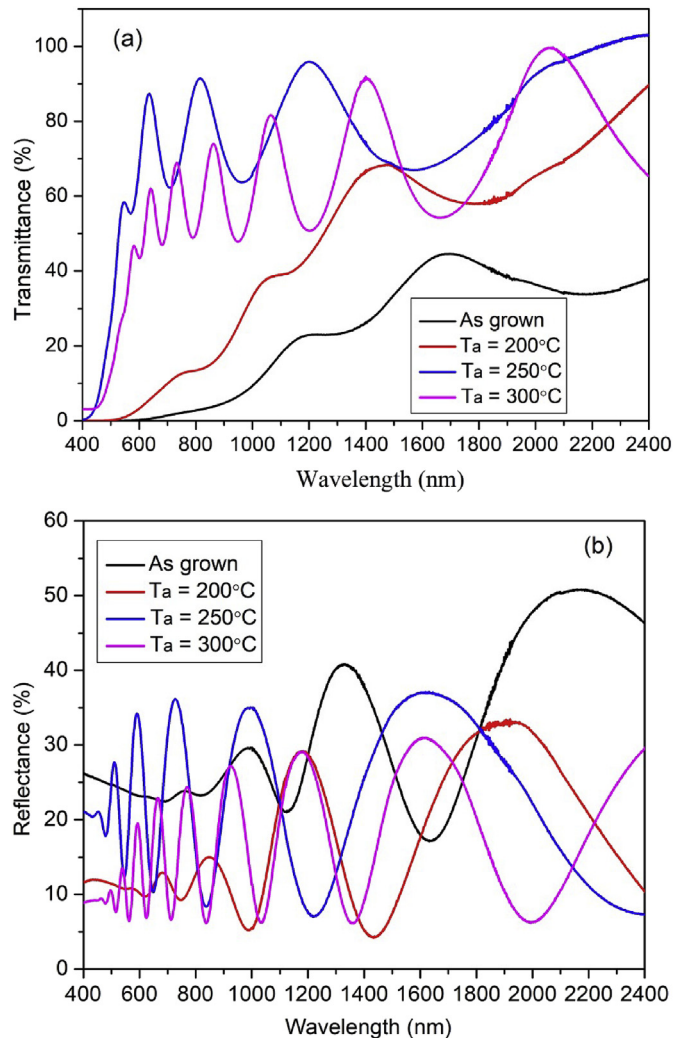As seen from Fig. 4 (a) the as-grown films and films annealed at 200 °C are poorly transparent in the visible region whereas for the films annealed at 250 °C and 300 °C good (> 70%) transmittance is observed as well as significant interference fringes are appeared. The last two features indicate an increase in homogeneity of the films and their crystalline quality [11].

The optical absorption coefficient (α) was calculated by the following equation [38]:

$$\alpha = -\frac{1}{t} ln \left(\frac{\sqrt{(1-R)^4 + 4T^2R^2} - (1-R)^2}{2TR^2} \right), \tag{6}$$

where t is the thickness of the films ($\sim 0.5\,\mu m$), T and R are the transmittance and reflectance, respectively.

Using the values of α and assuming that the band-to-band transition is direct allowed one can calculate the optical energy band gap (E_g) from the Tauc relation [39]:

$$(\alpha h\nu)^2 = A\,(h\nu - E_g), \tag{7}$$

where $h\nu$ is the incident photon energy, A is a constant.

The value of E_g was evaluated from the Tauc plot (see Fig. 5). The calculated E_g values were found to be 1.90 eV, 2.10 eV, 2.71 eV and 2.44 eV for as-grown and annealed at T$_a$ = 200 °C, 250 °C and 300 °C films, respectively. The observed enhancement of E_g upon annealing temperature increasing up to 250 °C was due to the improvement in the crystallinity and less defectiveness of the annealed films compared to the as-grown film [15]. The dynamics of E_g values with an increase of annealing temperature are in agreement with both GIXD analysis (Fig. 1) that showed the growth of (111) orientation of cubic phase and elemental analysis that revealed the closeness of S/In ratio to its stoichiometry (Table 3) at higher temperatures.

However, the films annealed at 300 °C showed some decrease in E_g due to the change in preferred orientation from (111) to (311) along with the simultaneous development of tetragonal β-In₂S₃ phase (Fig. 1). Moreover at this temperature, the stoichiometry of the films deviated
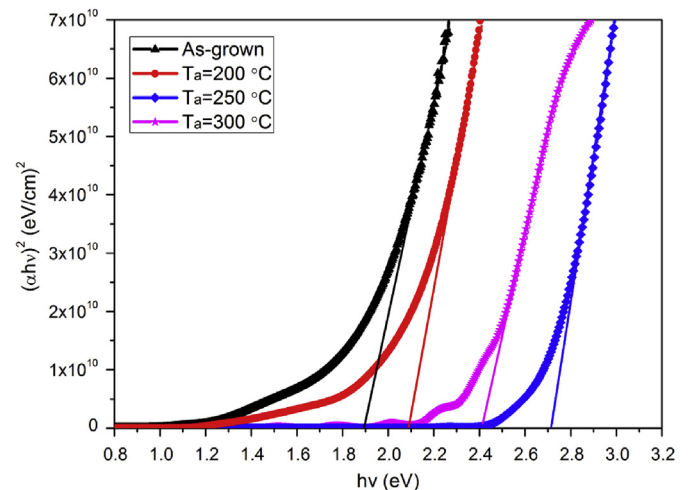

Fig. 4. (a) Transmission and (b) reflection spectra of In₂S₃ films.
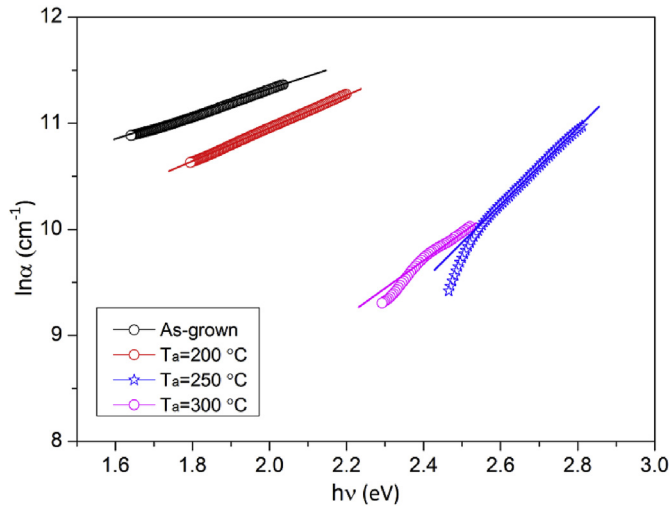

Fig. 5. Tauc plots for In₂S₃ films.

Fig. 6. Plot of ln(α) against photon energy (hν) for In$_2$S$_3$ films.

from the optimal value due to sulfur enrichment (Table 3), which results in decrease of band gap energy.

Further, to study the structural disorder of In$_2$S$_3$ films, the Urbach energy (E_U) was also calculated. The existence of an exponential increase in the absorption coefficient near the band edge (Urbach tail) indicates the presence of localized states or impurity states in the band gap region that causes disturbance in the band structure of the polycrystalline films [40]. The value of E_U indicates the level of crystallinity and structural defects present in the films. In the low photon energy range, an exponential variation in the absorption edge followed the Urbach empirical equation [41]:

$$\alpha = \alpha_0 \, exp\left[\frac{h\nu}{E_U}\right],$$ (8)

where α_0 is a constant.

The value of E_U can be obtained by linearization of the dependence of ln(α) on hν as given in Fig. 6 [42].

The determined E_U values for the corresponding In$_2$S$_3$ films decreased with increase of annealing temperature. The variation in Urbach energy and optical band gap energy with respect to annealing temperature is as shown in Fig. 7. The lower value of E_U at higher annealing temperatures indicates the decrease in structural disorder and density of localized states in the layers.
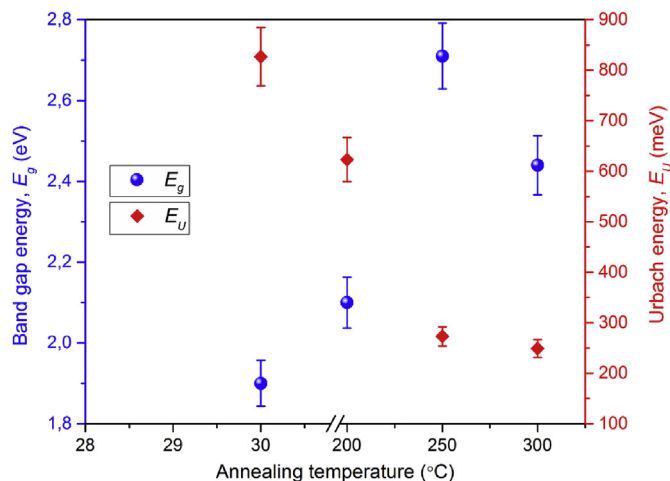

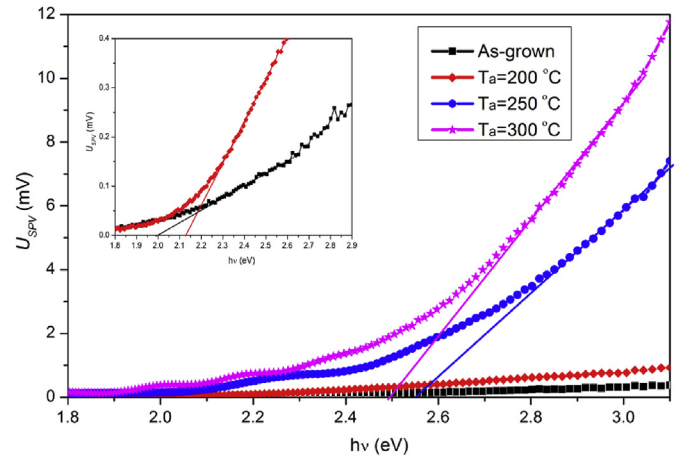**Fig. 7.** Variation of E_g and E_U with annealing temperature of In$_2$S$_3$ films.

Fig. 8. SPV signal versus photon energy of In$_2$S$_3$ films.

3.5. SPV studies

The positive SPV signal was obtained for all In$_2$S$_3$ films, indicating the n-type conductivity of the films [43]. Fig. 8 presents the spectral dependences of the SPV signal U_{SPV} for In$_2$S$_3$ films, annealed at different temperatures.

It was revealed that surface photovoltage generated from the films increases upon their annealing. The as-grown and films annealed at T$_a$ = 200 °C showed very low surface photovoltage compared to other annealed films. It may be caused by the presence of impurities' energy states or surface states in the band gap region, which allows high rate of recombination of photoinduced charge carriers that are generated at the surface. During annealing the concentration of impurity energy states or surface states are decreased, leading to a higher value of SPV signal and the increase in surface photovoltage is due to an increase of carrier concentration near the surface region. This increase in carrier concentration indicates increase in open circuit voltage, which is beneficial for the performance of the solar cell.

The SPV studies regarding the existence of surface states or tail states near the band edge region of the films are in accordance with the band bending analysis of Urbach tail, which was done through the optical absorption data (Fig. 6). It was revealed that the density of surface states and structural defects in In$_2$S$_3$ layers were decreased with increase of annealing temperature. In addition, the band gap of the films can be estimated from the SPV measurements as intersection of the extension of the curve with the hν-axis [44,45] as shown in Fig. 8. According to this, the determined band gap values of as-grown and films annealed at 200 °C, 250 °C and 300 °C are 1.99 eV, 2.12 eV, 2.55 eV and 2.49 eV respectively. The band gap energy increases with the annealing temperature as it was observed in Tauc plots (Fig. 5) and the values themselves are almost the same.

4. Conclusion

Changes occurred in the structural and optical behaviour of thermally evaporated In$_2$S$_3$ layers upon annealing in sulfur ambient have been investigated. The GIXD patterns revealed that the films are polycrystalline in nature and exhibited improved crystallinity with cubic structure of In$_2$S$_3$ and also the SEM images showed good uniformity and enhanced grain size with the raise of annealing temperature. The EDS analysis showed that S/In ratio increased with annealing temperature and the films annealed at 250 °C indicated composition close to stoichiometry. The energy band gap of the films increased while the Urbach energy values decreased with the increase of annealing temperature. The SPV data revealed that all the films had n-type conductivity and the obtained energy band gap values are in good agreement with the conventional optical data. The present work revealed that In$_2$S$_3$ films

annealed at 250 °C exhibited good structural properties, stoichiometry and surface morphology with a wide band gap compared to other layers and hence such films are suitable as window/buffer layer in the development of environmentally benign polycrystalline thin film solar cell.

Acknowledgements

References

[1] M.A. Mughal, R. Engelken, R. Sharma, Progress in indium (III) sulphide (In$_2$S$_3$) buffer layer deposition techniques for CIS, CIGS and CdTe-based thin film solar cells, Sol. Energy 120 (2015) 131.

[2] J.H. Kim, D. Shin, B.T. Ahn, Surface morphology control of In$_2$S$_3$ buffer layer by Sn incorporation and its application to cadmium-free Cu(In,Ga)Se$_2$ thin film solar cells, Curr. Appl. Phys. 16 (2016) 1040.

[3] X. Feng, Y. Chen, M. Wang, L. Guo, Hydrothermal synthesis of pyramid-like In$_2$S$_3$ film for efficient photoelectrochemical hydrogen generation, Int. J. Hydrogen Energy 42 (2017) 15085.

[4] Y.J. Hsiao, C.H. Lu, L.W. Ji, T.H. Meen, Y.L. Chen, H.P. Chi, Characterization of photovoltaics with In$_2$S$_3$ nanoflakes/p-Si heterojunction, Nanoscale Lett. 9 (2014) 32.

[5] N. Naghavi, S. Spiering, M. Powalla, B. Cavana, D. Lincot, High-efficiency copper indium gallium diselenide solar cells with indium sulfide buffer layers deposited by atomic layer chemical vapor deposition, Prog. Photovoltaics Res. Appl. 11 (2003) 437.

[6] R. Sáez-Araoz, J. Krammer, S. Harndt, et al., ILGAR In$_2$S$_3$ buffer layers for Cd-free Cu(In,Ga)(S,Se)$_2$ solar cells with certified efficiencies above 16%, Prog. Photovoltaics Res. Appl. 20 (2012) 855.

[7] P. Jackson, D. Hariskos, R. Wuerz, O. Kiowski, A. Bauer, T.M. Friedlmeier, M. Powalla, Properties of Cu(In,Ga)Se$_2$ solar cells with new record efficiencies up to 21.7%, Phys. Status Solidi RRL (2014) 1.

[8] Olivier Poncelet, Ratan Kotipalli, Bart Vermang, Angus Macleod, Laurent A. Francis, Denis Flandre, Optimization of rear reflectance in ultra-thin CIGS solar cells towards > 20% efficiency, Sol. Energy 146 (2017) 443.

[9] A.A. El Shazly, D. Abd Elhady, H.S. Metwally, M.A.M. Seyam, Electrical properties of β-In$_2$S$_3$ thin films, J. Phys. Condens. Mater. 10 (1998) 5943.

[10] P.M. Ratheesh Kumar, T. Theresa John, C. Sudha Kartha, K.P. Vijay Kumar, T. Abe, Y. Kashiwaba, Effect of thickness and post deposition annealing on the properties of evaporated In$_2$S$_3$ thin films, J. Mater. Sci. 41 (2006) 5519.

[11] A. Timouni, H. Bouzouita, M. Kanzari, B. Rezig, Fabrication and characterization of In$_2$S$_3$ thin films deposited by thermal evaporation technique, Thin Solid Films 480–481 (2005) 124.

[12] S. P Nehra, S. Chander, A. Sharma, M.S. Dhaka, Effect of thermal annealing on physical properties of evaporated In$_2$S$_3$ buffer layer for eco-friendly photovoltaic applications, Mater. Sci. Semicond. Process. 40 (2015) 26.

[13] A. Timoumi, H. Bouzouita, R. Brini, M. Kanzari, B. Rezig, Optimization of annealing conditions of In$_2$S$_3$ thin films deposited by vacuum thermal evaporation, Appl. Surf. Sci. 253 (2006) 306.

[14] M.M. El-Nahass, B.A. Khalifa, H.S. Soliman, M.A.M. Seyam, Crystal structure and optical absorption investigations on β-In$_2$S$_3$ thin films, Thin Solid Films 515 (2006) 1796.

[15] N. Revathi, P. Prathap, R.W. Miles, K.T.R. Reddy, Annealing effect on the physical properties of evaporated In$_2$S$_3$ films, Sol. Energy Mater. Sol. Cells 94 (2010) 1487.

[16] K. Bouabid, A. Ihlal, Y. Amira, A. Sdaq, A. Outzourhit, G. Nouet, Effect of annealing on In$_2$S$_3$ thin films prepared by flash evaporation, Eur. Phys. J. Appl. Phys. 40 (2007) 149.

[17] R. Ranjith, T. Theresa John, C. Sudha Kartha, K.P. Vijaykumar, T. Abe, Y. Kashiwaba, Post-deposition annealing effect on In$_2$S$_3$ thin films deposited using SILAR technique, Mater. Sci. Semicond. Process. 10 (2007) 49.

[18] M. Bedir, M. Oztas, Effect of air annealing on the optical, electrical and structural properties of In$_2$S$_3$ films, Sci. China Ser. E Tech. Sci. 51 (2008) 487.

[19] C. Sanz, C. Guillén, J. Herrero, Annealing of indium sulfide thin films prepared at low temperature by modulated flux deposition, Semicond. Sci. Technol. 28 (2013) 015004.

[20] A. Omelianovych, J.H. Kim, L. Liudmila, B.T. Ahn, Effect of post annealing on the characteristics of In$_2$S$_3$ buffer layer grown by chemical bath deposition on a CIGS substrate, Curr. Appl. Phys. 15 (2015) 1641.

[21] B. Yahmadi, N. Kamoun, R. Bennaceur, M. Mnari, M. Dachraoui, K. Abdelkrim, Structural analysis of indium sulfide thin films elaborated by chemical bath deposition, Thin Solid Films 473 (2005) 201.

[22] B.A. Senjo, A.M. Chaparro, M.T. Gutierrez, J. Herrero, C. Maffiotte, Study of the electrodeposition of In$_2$S$_3$ thin films, Thin Solid Films 480–481 (2005) 151.

[23] J.F. Trigo, B. Asenjo, J. Herrero, M.T. Gutiérrez, Optical characterization of In$_2$S$_3$ solar cell buffer layers grown by chemical bath and physical vapour deposition, Sol. Eng. Mater. Sol. Cells 92 (2008) 1145.

[24] A. Timouni, H. Bouzouita, B. Rezig, Optical constants of Na-In$_2$S$_3$ thin films prepared by vacuum thermal evaporation technique, Thin Solid Films 519 (2011) 7615.

[25] T. Sall, B.M. Soucase, M. Mollar, B. Hartitti, M. Fahoume, Chemical spray pyrolysis of β-In$_2$S$_3$ thin films deposited at different temperatures, J. Phys. Chem. Solid. 76 (2015) 100.

[26] L. Kronik, Y. Shapira, Surface photovoltage phenomena: theory, experiments and applications, Surf. Sci. Rep. 37 (1999) 1.

[27] D. Cavalcoli, A. Cavallini, Surface photovoltage spectroscopy – method and applications, Phys. Status Solidi C 7 (2010) 1293.

[28] D. Cavalcoli, B. Fraboni, A. Cavallini, Surface photovoltage spectroscopy analyses of Cd$_{1-x}$Zn$_x$Te, J. Appl. Phys. 103 (2008) 043713.

[29] D. Cavalcoli, B. Fraboni, A. Cavallini, Chapter seven – surface and defect states in semiconductors investigated by surface photovoltage, Semiconduct. Semimet. 91 (2015) 251.

[30] K.L. Chopra, Thin Film Phenomena, McGraw-Hill, New York, 1969, p. 163.

[31] N. Revathi, P. Prathap, K.T. Ramakrishna Reddy, Thickness dependent physical properties of close space evaporated In$_2$S$_3$ films, Solid State Sci. 11 (2009) 1288.

[32] J. Raj Mohamed, L. Amalraj, Effect of precursor concentration on physical properties of nebulized spray deposited In$_2$S$_3$ thin films, J. Asian Ceram. Soc. 4 (2016) 357.

[33] M.G. Sandoval-Paz, M. Sotelo-Lerma, J.J. Valenzuela-Ja´uregui, M. Flores-Acosta, R. Ramirez-Bon, Structural and optical studies on thermal-annealed In$_2$S$_3$ films prepared by the chemical bath deposition technique, Thin Solid Films 472 (2005) 5.

[34] B.E. Warren, X-ray Diffraction, Dover, New York, 1990, p. 253.

[35] G.K. Williamson, R.E. Smallman III., Dislocation densities in some annealed and cold-worked metals from measurements on the X-ray Debye-Scherrer spectrum, Philos. Mag. A 1 (1956) 34.

[36] A. Purohit, S. Chander, S.P. Nehra, M.S. Dhaka, Effect of air annealing on structural, optical, morphological, and electrical properties of thermally evaporated CdSe thin films, Physica E 69 (2015) 342.

[37] Z.Y. Zhong, E.S. Cho, S.J. Kwon, Effect of substrate temperatures on evaporated In$_2$S$_3$ thin film buffer layers for Cu(In,Ga)Se$_2$ solar cells, Thin Solid Films 547 (2013) 22.

[38] D.K. Shroder, Semiconductor Materials and Device Characterization, Wiley, New York, 1990.

[39] J. Tauc, Optical Properties of Solids, North-Holland, Amsterdam, 1970, p. 903.

[40] R.H. Parmenter, Energy levels of a disordered alloy, Phys. Rev. 97 (1955) 587.

[41] J. Melsheimer, D. Ziegler, Band gap energy and Urbach tail studies of amorphous, partially crystalline and polycrystalline tin dioxide, Thin Solid Films 129 (1985) 35.

[42] A.S. Hassanien, A.A. Akl, Effect of Se addition on optical and electrical properties of chalcogenide CdSSe thin films, Superlattice. Microst. 89 (2016) 153.

[43] L. Kronik, Y. Shapira, Surface photovoltage spectroscopy of semiconductor structures: at the crossroads of physics, chemistry and electrical engineering, Surf. Interface Anal. 31 (2001) 954.

[44] M. Pomaska, R. Sáez-Araoz, A. Steigert, Y.P. Fu, F. Hergert, I. Lauermann, T. Dittrich, M. Lux-Steiner, C.H. Fischer, Influence of Cl and H$_2$O in spray-ILGAR solutions on the voltage gain of Cu(In,Ga)(S,Se)$_2$ solar cells with In$_2$S$_3$ buffer, Sol. Eng. Mater. Sol. Cells 132 (2015) 303.

[45] N.E. Gorji, U. Reggiani, L. Sandrolini, Surface photovoltage spectroscopy and AFM analysis of CIGSe thin film solar cells, Int. J. Photoenergy (2015) 8295301.